Analysis of the aerodynamic loads on a wind turbine in off-design conditions

G. Santo, M. Peeters, W. Van Paepegem and J. Degroote

Key words: Wind energy, atmospheric boundary layer, wind turbine, off-design.

Abstract In this work, the aerodynamic loads acting on a large horizontal axis wind turbine are analysed in off-design conditions by means of computational fluid dynamics (CFD) simulations. The turbulent wind flow is solved using an unsteady RANS approach and choosing the $k-\epsilon$ model. Appropriate boundary conditions are used in combination with modified wall functions in order to preserve the atmoshperic boundary layer (ABL) profiles throughout the entire domain. An overset technique is used to handle the rotation of the blades throughout the simulated time. Changing both the pitch angle of the blades and the tip-speed ratio (TSR) of the turbine, several operating points are investigated. The performance and the loads are highly affected by the ABL, whose effect is highlighted. The performance of the wind turbine in each simulated operating point is compared to the nominal operating point (NOP). The aerodynamic loads are monitored, analysed and mutually compared throughout the motion of the rotor, in order to identify the most critical conditions for the blade structures.

Gilberto Santo
Department of Flow, Heat and Combustion Mechanics, Ghent University. Sint-Pietersnieuwstraat 41 - 9000 Ghent (Belgium), e-mail: gilberto.santo@ugent.be

Mathijs Peeters
Department of Materials Science and Engineering, Ghent University, Technologiepark-Zwijnaarde 903 - 9052 Zwijnaarde (Belgium), e-mail: mathijs.peeters@ugent.be

Wim Van Paepegem
Department of Materials Science and Engineering, Ghent University, Technologiepark-Zwijnaarde 903 - 9052 Zwijnaarde (Belgium), e-mail: wim.vanpaepegem@ugent.be

Joris Degroote
Department of Flow, Heat and Combustion Mechanics, Ghent University. Sint-Pietersnieuwstraat 41 - 9000 Ghent (Belgium), e-mail: joris.degroote@ugent.be

1 Introduction

In the last decades, large efforts have been made to explore alternative techniques to replace fossil fuels as energy source. In particular, among renewable energies, wind energy plays an increasingly important role. Given the aleatory nature of the wind, wind turbines are designed to function in a wide range of operating conditions [1]. For this reason, their operation has to be adapted to face the incoming wind and adapt the output power accordingly. Normally, in large horizontal axis wind turbines, this is achieved by pitching the blades (i.e. rotating them around their own axes) and/or changing the tip speed ratio. These controlling techniques can be investigated in detail by means of computational fluid dynamics (CFD). Sudhamshu et al. [2] carried out CFD (steady RANS) simulations of the NREL Phase VI wind turbine, modelling only one blade and changing both the incoming constant wind speed and the blade pitch angle. Li et al. [3] adopted an overset technique to simulate the aerodynamics of a wind turbine and investigate the effect of various wind speeds and pitch angles on the transient response of the machine. In literature, the effect of the atmospheric boundary layer (ABL) i.e. wind speed increasing with height, is often neglected. Nevertheless, this is expected to induce large differences in the forces acting on each blade during its rotation, also due to the tendency of upscaling the size of modern machines [4].

In this work, a commercial 3-bladed rotor with a diameter of 100 m is modelled by an overset technique, together with its supporting structures, namely tower and nacelle. The whole machine is immersed in the ABL flow, which leads to a wind speed increasing with height. Various operating points in the surrounding of the nominal operating point (NOP) are simulated by changing the pitch angle of the blades and the tip-speed ratio. Both the energy conversion performance of the turbine and the loads acting on the blades will be analysed in detail during the transient rotation of the machine.

2 Methodology

The domain of the flow simulation is displayed in fig. 1, with indication of the boundary conditions. A distance equal to 5 rotor diameters from the top and side symmetry surfaces is chosen in order to avoid artificial acceleration of the flow. Furthermore, the inflow and the outflow are respectively 5 and 15 rotor diameters away from the rotor.

A 3D fully hexahedral mesh is created for every component of the machine, namely the 3 blades, the hub, the nacelle and the tower. These meshes are then overlapped to a fully structured background mesh and the mutual connectivity is established by means of an overset technique [3, 5]. Fig. 2 shows the details of the mesh around each blade, together with an overview of the adopted overset technique. The total number of cells is approximately 56 millions, with 49.6 million cells in

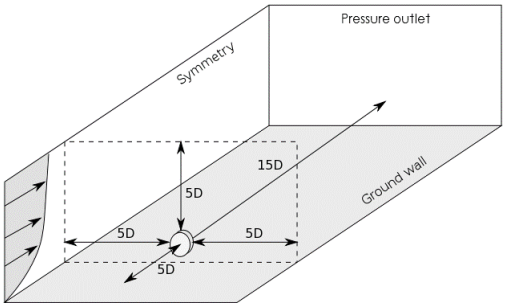

Fig. 1 Simulation layout with the cylinder in the center denoting the domain around the rotor, with diameter D = 100 m.

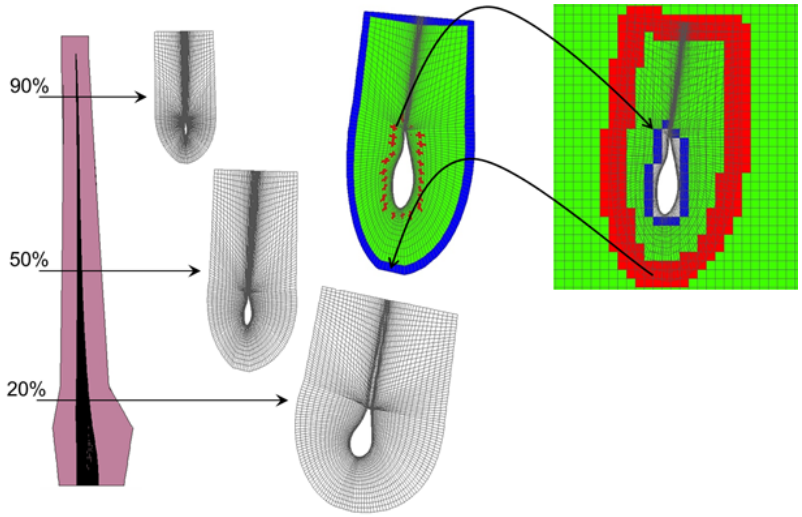

Fig. 2 (left) sections of the blade component mesh at different spanwise locations and (right) illustration of the mesh connectivity strategy: solve cells are marked in green, donor cells in red and receptor cells in blue.

the background mesh and the rest belonging to the component meshes (blades, hub, tower and nacelle).

As an example of how the mesh connectivity is built, the connection of the blade mesh with the background grid is shown in fig. 2. The background cells encompassed or crossed by the blade walls are deactivated. On the external boundary of the component mesh, the solution is obtained by interpolation from the background mesh. Here, the two meshes are designed to have roughly the same cell size (i.e. edge size around 0.275 m). The (background) cells from where the solution is taken are marked as “donor cells”, while the (component) cells receiving solution by interpolation are marked as “receptor cells”. At least 4 donor cells contribute to interpolation on each receptor cell.

The fluid is modelled as incompressible and turbulence is represented by means of the $k-\epsilon$ model. At the inlet of the domain, the velocity, turbulent kinetic energy and dissipation rate distributions are prescribed to mimic the distribution of a neutral ABL. The profiles first proposed by Richard and Hoxey [6] are adopted. They are summarized in equations 1, 2 and 3.

$$u(z) = \frac{u_*}{K} ln\left(\frac{z+z_0}{z_0}\right) \tag{1}$$

$$k = \frac{u_*^2}{\sqrt{C_\mu}} \tag{2}$$

$$\epsilon(z) = \frac{u_*^3}{K(z+z_0)} \tag{3}$$

In these equations, u is the wind velocity as a function of the height z, u_* is the friction velocity (an index of the intensity of the wind), z_0 is the aerodynamic roughness length (which provides an estimation of the roughness of the ground wall) and k and ϵ are respectively the turbulent kinetic energy and its dissipation rate. Furthermore, K is the von Karman constant (0.42) and C_μ is a constant of the turbulence model, set to 0.09 [7]. In order to consistently sustain and preserve the inlet profiles across the whole computational domain, a new formulation for the ground wall functions is necessary [8, 9, 10]. Thus, following the approach of Parente and Benocci [8], the aerodynamic roughness length is directly included in the wall functions, leading to a modified non-dimensional wall distance z^+ and a modified wall function constant E.

$$z^+_{mod} = \frac{(z+z_0)u_*\rho}{\mu} \tag{4}$$

$$E_{mod} = \frac{\mu}{\rho z_0 u_*} \tag{5}$$

These modified wall functions are used on the ground wall (fig. 1), while the standard ones are used on every other wall. In this work, the friction velocity is set to $u_* = 0.67\,m/s$ and the aerodynamic roughness is set to $z_0 = 0.5\,m$, leading to a wind speed of $8.5\,m/s$ at the hub height ($100\,m$). This is the nominal wind velocity provided by the blade manufacturer. The turbulent kinetic energy is set to $0.015\,m^2/s^2$, leading to a turbulence intensity of approximately 1.25% at the hub height. The momentum equations and continuity equation are solved together in a pressure-based solver. Second-order upwind discretization for momentum is applied and a first-order implicit scheme is used for time discretization. The tip-speed ratio (TSR) to be used in this work is defined as the ratio of the speed of the blade tip u_{tip} and the undisturbed wind velocity at hub height v_{hub}. The blade speed at the tip can be computed as the product of the rotational speed ω and the blade length R, according to:

$$TSR = \frac{u_{tip}}{v_{hub}} = \frac{\omega R}{v_{hub}} \tag{6}$$

The nominal operating point, as provided by the blade manufacturer, corresponds to a TSR of 8.5 and a pitch angle taken as reference and marked as “pitch 0”. Around this point, 8 more points are analyzed, changing both the TSR and the pitch angle of the blades. The rotational speed of the turbine is changed in order to change its tip speed ratios, as summarized by table 1.

Table 1 Analyzed tip speed ratios and respective rotational speed.

TSR	Rotational Speed
7.5	1.275 rad/s
8.5	1.445 rad/s
9.5	1.615 rad/s

Independently of the TSR to be simulated, each full rotation of the wind turbine rotor is divided into 240 time steps. For each of these TSRs, 3 different blade pitch angles are simulated: the pitch “0 degree”, the pitch “+2 degrees” and the pitch “-2 degrees”. The last two are obtained by rotating the blades of +2 degrees or -2 degrees around their axis (positive rotation corresponding to a nose-down rotation of each section). This leads to a total of 9 simulations carried out. First, the turbine rotation is started in the unperturbed ABL, considering a TSR of 8.5 for each analyzed pitch angle. Then, after 5 complete rotations, the TSR is changed to the desired value and additional full rotations (from 2 to 7) are carried out until the torque provided by the machine stabilizes (i.e. difference between the last two thirds of revolution smaller than 1.8%). Finally, only the last revolution is analyzed. Running on 280 cores (10 nodes, each with 2 CPUs of the type 14-core Xeon E5-2680v4, 2.4GHz, inter-connected via InfiniBand), approximately one day is necessary to perform a complete revolution.

3 Results

In this section, the energy conversion performance of the turbine in each of the simulated operating points will be analyzed, before examining the loads acting on each blade. The torque coefficient c_T and the power coefficient c_P to be used, are defined according to:

$$c_T = \frac{Torque}{\frac{1}{2}\rho v^2 AR} \tag{7}$$

$$c_P = \frac{Power}{\frac{1}{2}\rho v^3 A} = c_T \cdot TSR \tag{8}$$

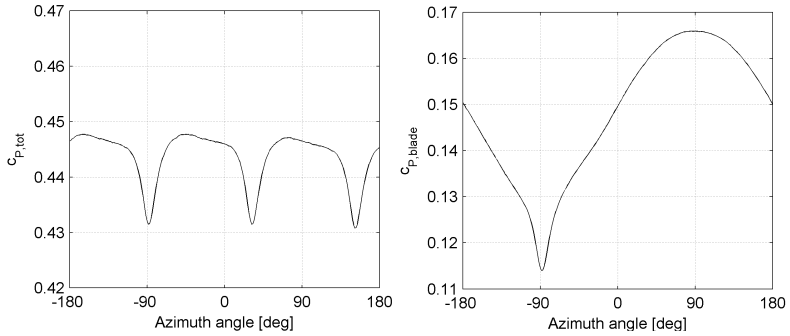

Fig. 3 (left) total power coefficient and (right) single blade contribution to the total power as a function of the azimuth angle.

In these equations, ρ is the constant density of air ($1.225\ kg/m^3$), v is the undisturbed wind speed at the hub height ($8.5\ m/s$), R the radius of the rotor ($50\ m$) and A its frontal area. Furthermore, to define the position of each blade during the rotation, the 0 azimuth angle position corresponds to the blade horizontally positioned and in uprising motion. Thus, +90 degrees azimuth angle corresponds to the blade pointing upwards and -90 degrees to the blade pointing downwards and passing in front of the tower.

For every operating point, qualitatively the same curve is observed for the extracted power during the last monitored revolution. Fig. 3-left reports the total power at the NOP, as a function of the azimuth angle of one of the three blades. On the other hand, fig. 3-right shows the power contribution of each blade. Note that, in both plots, a drop is visible in the power produced whenever a blade passes in front of the tower. This phenomenon is addressed as “tower dam" and results from the pressure increase induced by the tower obstruction on the suction side of the blade. The single blade contribution is largely influenced by the ABL, producing more power when the blade points upwards (and where the ABL induces higher wind speed) and less when it points downwards (where the ABL induces lower wind speeds). This results in a peak-to-peak amplitude of about 36% of the average value at NOP. Nevertheless, the combination of the three blades produces a stable total power coefficient, which exhibits a maximum deviation from its average lower than 3%.

Qualitatively the same curves can be obtained for every operated point. Fig. 4-left shows the average power coefficient obtained for all the examined operating points. It is reported that the operating point corresponding to +2 degrees pitch and 9.5 TSR has a higher power coefficient (+4.7%) than the nominal operating point provided by the manufacturer. When simulating these two particular operating points, the difference in power coefficient between the last two third of revolution (used to assess convergence towards time regime) is, in both cases, lower than 0.3%. It is therefore concluded that the differences observed are larger than the margin of error of the simulations. On the other hand, every other operating point exhibits a lower coefficient (up to -18.6% for -2 degrees pitch and 9.5 TSR) with respect to the NOP.

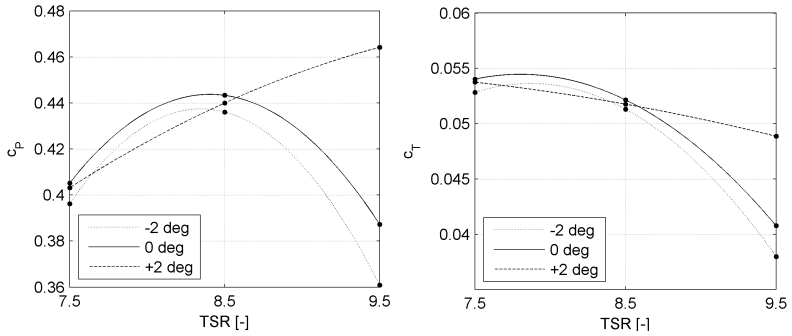

Fig. 4 Average values of (left) total power coefficient and (right) total torque coefficient of the turbine for all the simulated operating points.

However, fig. 4-right reports the torque coefficient corresponding to all the analyzed operating points. From equation 8 it can be seen that the power coefficient results from the product of the TSR and the torque coefficient. For every pitch angle, an increase in TSR leads to a decrease in torque coefficient, since the angle of attack on the blade decreases. When the pitch angle is changed, the distribution of the angle of attacks over the entire blade span is shifted. This leads to a different operation of each airfoil lofted along the blade and, additionally, to different directions of the produced lift and drag forces. Consequently, the (positive) contribution of the lift and the (negative) contribution of the drag will combine differently to the produced torque, according to the adopted pitch angle and TSR. The best performing point visible in fig. 4-left provides a lower torque coefficient compared to the NOP. Nevertheless, the increase in rotational speed (i.e. in TSR) is stronger than the reduction in c_T, leading to an overall higher power coefficient.

A similar analysis can be carried out for the axial load acting on each blade. The axial force is in fact the highest force component and it is the one dominantly contributing to the deflection of the blades during the operation of the machine. The axial force acting on each blade can be related directly to its position. Being largely influenced by the ABL and by the tower-dam effect, a similar plot of fig. 3-right can be obtained also for the axial force acting on each blade. Fig. 5-left shows the average value of the axial force, while fig. 5-right shows the peak-to-peak amplitude, which directly relates to the arising of fatigue problems. Note that, differently than what is observed for the torque, the average axial force consistently increases with increasing TSR, following the increase in incoming velocity magnitude more than the decrease in angle of attack. A similar behavior is observed also by other authors [11]. The point previously highlighted for having a higher c_P than the NOP also shows a slightly smaller average axial force (-1.7%), but, at the same time, is also the one with the highest amplitude in its oscillation. The operating point with -2 degrees pitch and 9.5 TSR has the highest average value of the axial force (+24.7% when compared to NOP).

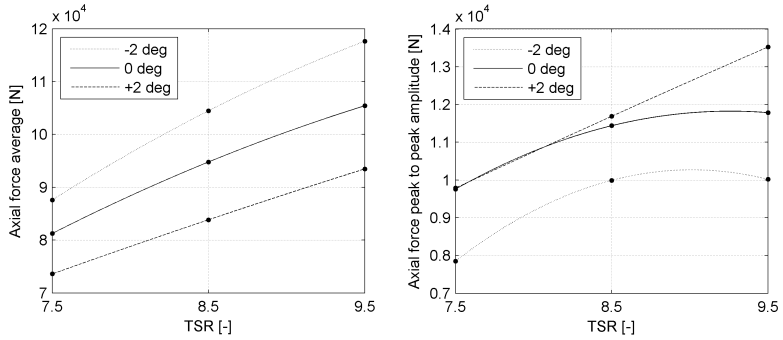

Fig. 5 (left) Average values and (right) peak to peak amplitudes of the axial force acting on each blade.

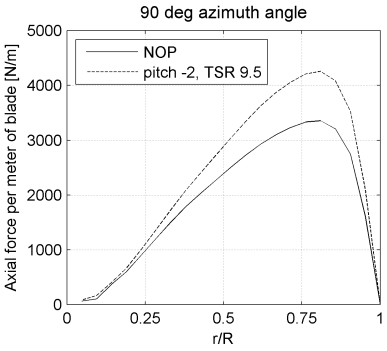

Fig. 6 Distributions of axial force per meter of blade as a function of the blade span, at 90 degrees azimuth angle, namely the highest load condition.

The distribution of the axial force throughout the blade can also be analyzed as done in fig. 6. A consistent increase of the axial force solicitation is monitored throughout the entire blade span and the highest increase is observed at about 75% of the radius, where the axial force also reaches its peak. A similar condition is reported during the entire rotation.

4 Conclusions

Changing the blade pitch angle and its tip speed ratio, 9 operating points were simulated, keeping the ABL wind flow unchanged. In this way, the characteristic of the turbine has been built in the proximity of the nominal operating point (NOP). A better performing point could be identified.

The axial force average value and amplitude of oscillation were also monitored, showing that the previously identified better performing point is characterized by a

higher amplitude of the oscillating axial force on each blade. Furthermore, one of the operating points exhibited an average value of the axial force 24.7% higher than at the NOP. This increase is spread over the entire blade span, reaching its maximum at about 75% of its span.

Following the present work, the operating point with the highest observed axial force will be simulated in a fluid-structure interaction framework developed by the same authors [12], in order to investigate the structural response of the blades in unfavorable off design conditions.

References

1. E. Hau. "Wind Turbines: fundamentals, Technologies, Application, Economics" (2nd Edition). Springer: Berlin, 2006
2. A.R. Sudhamsu, M.C. Pandey et al. Numerical study of effect of pitch angle on performance characteristics of a HAWT. Engineering Science and Technology, an International Journal, 2016. DOI: 10.1016/j.jestch.2015.09.010
3. Y. Li, K.J. Paik, T. Xing, P. M. Carrica. Dynamic overset CFD simulations of wind turbine aerodynamics. Renewable Energy, 2012. DOI: 10.1016/j.renene.2011.06.029
4. M. Caduff, M.A.J. Huijbregts, H.J. Althaus, A. Koehler, S. Hellweg. Wind power electricity: the bigger the turbine, the greener the electricity? Environmental Science and Technology, 2012. DOI: 10.1021/es204108n
5. F. Zahle, N.N. Sørensen and J. Johansen. Wind turbine rotor-tower interaction using an incompressible overset grid method. Wind Energy 2009. DOI: 10.1002/we.327
6. P.J. Richards, R.P. Hoxey. Appropriate boundary conditions for computational wind engineering models using the $k - \epsilon$ turbulence model. Journal of Wind Engineering and Industrial Aerodynamics, 46 and 47, 145-153, 1993.
7. B. E. Launder, D. B. Spalding. "Lectures in Mathematical Models of Turbulence". Academic Press, London, 1972
8. A. Parente, C. Gorlè, J. van Beeck, C. Benocci. A Comprehensive Modelling Approach for the Neutral Atmospheric Boundary Layer: Consistent Inflow Conditions, Wall Function and Turbulence Model. Boundary Layer Meteorology, 2011. DOI: 10.1007/s10546-011-9621-5
9. B. Blocken, T. Stathopoulos, J. Carmeliet. CFD simulation of the atmospheric boundary layer: wall function problems. Atmospheric Environment, 2017. DOI: 10.1016/j.atmosenv.2006.08.019
10. A. Parente, C. Gorlè, J. van Beeck, C. Benocci. Improved $k - \epsilon$ model and wall function formulation for the RANS simulation of ABL flows. Journal of Wind Engineering and Industrial Aerodynamics, 2011. DOI: 10.1016/j.jweia.2010.12.017
11. L. Dai, Q. Zhou, Y. Zhang, S. Yao, S. Kang, X. Wang. Analysis of wind turbine blades aeroelastic performance under yaw conditions. Journal of Wind Engineering and Industrial Aerodynamics, 2017. DOI: 10.1016/j.jweia.2017.09.011
12. G. Santo, M. Peeters, W. Van Paepegem, J. Degroote. Transient aeroelastic simulations of wind turbines with composite blades. In proceedings of the 7th GACM Colloquium on Computational Mechanics for Young Scientists from Academia and Industry, 2017.